IMPROVEMENT OF READHESION CONTROL OF AN ELECTRIC RAILWAY VEHICLE BY USING MULTIRATE SAMPLING OBSERVER

Lilit Kovudhikulrungsri*[1], Daisuke Tateishi*[2] and Takafumi Koseki*[3]

*[1] *Department of Electrical Engineering, The University of Tokyo, lilit@koseki.t.u-tokyo.ac.jp*
*[2] *Department of Electrical Engineering, The University of Tokyo, tateishi@koseki.t.u-tokyo.ac.jp*
*3 *Department of Information and Communication, The University of Tokyo, koseki@koseki.t.u-tokyo.ac.jp*

ABSTRACT

This paper proposes an effective way to improve readhesion control of traction drives. To do this, multirate sampling observers are introduced to all axles in order to estimate precise speed and load torque at every sampling instant. The slip-slide is detected by using the amount of the load torque correction estimated from the multirate sampling observer, which is insensitive to the effect of slope. The performance of the proposed control scheme is verified by comparing with the conventional method.

1. INTRODUCTION

Adhesion problem between rail and wheels is a major problem of traction control since the adhesion characteristic always varies with the velocity, temperature, humidity, rail condition, etc. The adhesion characteristic is expressed in the form of the adhesive coefficient. When a train runs from a high adhesive section into a low adhesive section, slip-slide takes place. As a result, the train's acceleration or deceleration drops abruptly. For this reason, it is necessary to apply some control method to bring it back to the adhesive condition. This control method is called readhesion control.

To realize an effective readhesion control, fast slip-slide detection must be implemented. The slip-slide is detected conventionally by using the acceleration of each wheel. In Japanese train, the acceleration of each wheel is detected by using a pulse generator, PG, of which output is the angle of the shaft. This information is differentiated twice in order to obtain the wheel's acceleration. However, since the pulse generators installed in Japanese trains have low resolutions (normally 60 pulses per revolution), the pulses cannot be achieved frequently at low speed. For example, in case of a Japanese train of which the wheel radius is 430 mm, if the control period is set to 0.2 ms, the pulse from the PG cannot be detected when the train speed drops below 53.5 km/h. As a result, it is necessary to extend the control period of the processor, but this method will finally result in slow readhesion control.

This paper is separated into two parts. In the first part, we describe a multirate sampling observer, which can solve the problem of low resolution by estimating a precise speed at every processor's sampling time, and effectiveness by comparison with the conventional numerical differentiation method. The multirate sampling observer is then applied to each axle of the train in the second part for slip-slide detection and readhesion control.

2. MULTIRATE SAMPLING OBSERVER

As stated in the previous section, it is necessary to estimate the speed and acceleration at every sampling time in order to achieve precise control. A conventional single-rate-discrete-time observer, which estimates and corrects the error at every sampling instant, is not suitable for this application. For this result, we introduce the multirate sampling observer, which estimates the state variables at every sampling time but corrects the error only when a pulse from the PG is detected, to the system. The block diagram of the multirate sampling observer is illustrated in Fig. 1.

2.1 Derivation of the Multirate Sampling observer

Derivation of the multirate sampling observer is based on the timing diagram in Fig. 2, where T_1 is the interval between the pulses, T_2 is the control of sampling period, m is the number of the pulse and n is the number of the

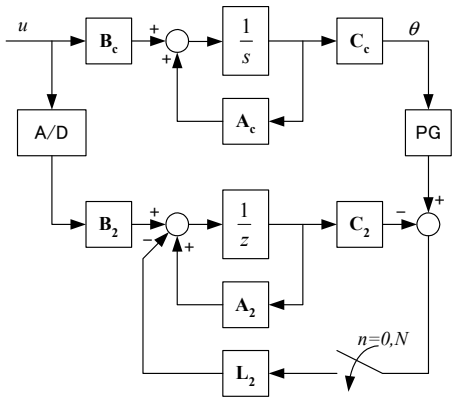

Fig.1 Block diagram of the multirate sampling observer

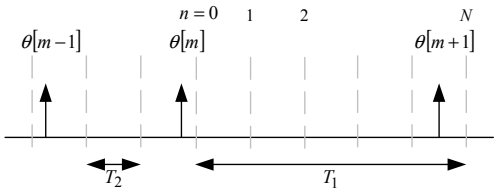

Fig.2 Timing diagram

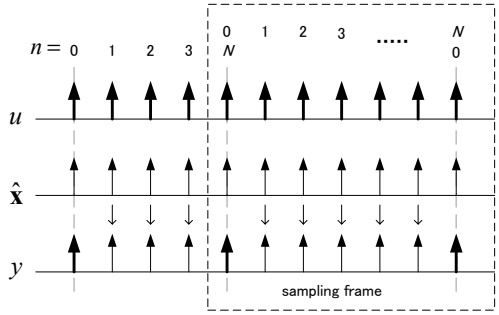

Fig.3 Discrete time signals

sampling instant after the pulse is detected. The observer is derived from a speed observer in discrete-time domain with disturbance dynamics consideration.

$$\hat{\mathbf{x}}[n+1] = (\mathbf{A_2} - \mathbf{L_2}\mathbf{C_2})\hat{\mathbf{x}}[n] + \mathbf{B_2}u[n] + \mathbf{C_2}y[n], \quad (1)$$

where $\hat{\mathbf{x}} = \begin{bmatrix} \hat{\theta} & \hat{\omega} & \hat{T}_L & \hat{\dot{T}}_L \end{bmatrix}^T$, $u = T_m$ and $y = \theta$. θ, ω, T_L and T_m represent shaft angle, motor speed, load torque and motor torque, respectively. $\mathbf{L_2}$ is the observer gain matrix. Note that the input u and the output y in this case are scalars quantities, but generally they can be vectors based on the state space description. The subscript 2 indicates that the constant DSP clock T_2 is used as the sampling time of the system and the symbol ^ indicates the estimated value. Matrices $\mathbf{A_2}$, $\mathbf{B_2}$ and $\mathbf{C_2}$ are derived from their continuous time domain matrices with disturbance consideration $\mathbf{A}$, $\mathbf{B}$ and $\mathbf{C}$, respectively. The components of these matrices are described as follow

$$\mathbf{A} = \begin{bmatrix} 0 & 1 & 0 & 0 \\ 0 & 0 & 1/J & 0 \\ 0 & 0 & 0 & 1 \\ 0 & 0 & 0 & 0 \end{bmatrix}, \mathbf{B} = \begin{bmatrix} 0 \\ 1/J \\ 0 \\ 0 \end{bmatrix}, \mathbf{C} = \begin{bmatrix} 1 & 0 & 0 & 0 \end{bmatrix}, \quad (2)$$

where J is the moment of inertia of the rotating part. The plant in this case is only the mechanical dynamics of the single rotating part including the motor and the wheels, which can be described as follow

$$\mathbf{A_c} = \begin{bmatrix} 0 & 1 \\ 0 & 0 \end{bmatrix}, \quad \mathbf{B_c} = \begin{bmatrix} 0 \\ 1/J \end{bmatrix}, \quad \mathbf{C_c} = \begin{bmatrix} 1 & 0 \end{bmatrix}, \quad \mathbf{x} = \begin{bmatrix} \theta \\ \omega \end{bmatrix}. \quad (3)$$

Fig. 3 shows a diagram of discrete time signals. Thick arrows represent actual values and thin arrows stand for estimated values. We define periods between the detected pulses as sampling frames. Hence, the interval of each sampling frame has the period of T_1. From the diagram, the actual output y or the shaft angle can be obtained only when an encoder pulse is detected. At this moment, the error of estimation is corrected. On the other hand, when pulses are not detected, the observer principally works as a simulator, calculating the state variables based on the plant model. This condition is achieved by using the estimated shaft angle when the detected pulses are not available as illustrated in the diagram. This method is practical in both simulations and experiments since it can be programmed easily. This leads to the assumption that

$$y = \begin{cases} y, & n = 0, N; N = T1/T2 \\ \hat{y}, & \text{otherwise} \end{cases}, \quad (4)$$

where n is the sampling index in each sampling frame, N is the last sampling instant in each frame. Hence, the observer equations can be expressed as follow

$$n = 0, N; \quad \hat{\mathbf{x}}_{n+1} = \mathbf{A_2}\hat{\mathbf{x}}_n + \mathbf{B_2}u_n + \mathbf{L_2}(y_n - \hat{y}_n), \quad (5)$$

$$n \neq 0, N; \quad \hat{\mathbf{x}}_{n+1} = \mathbf{A_2}\hat{\mathbf{x}}_n + \mathbf{B_2}u_n. \quad (6)$$

Due to this fact, the last sampling instant in each sampling frame decides the dynamics of the next sampling frame. Dynamics of each frame can be expressed by

$$\hat{\mathbf{x}}_\mathbf{n} = \mathbf{A_2}^{n-1}(\mathbf{A_2} - \mathbf{L_2}\mathbf{C_2})\hat{\mathbf{x}}_0 + \mathbf{A_2}^{n-1}\mathbf{B_2}u_0 + \mathbf{A_2}^{n-2}\mathbf{B_2}u_1 + \cdots + \mathbf{A_2}^0\mathbf{B_2}u_{n-1} + \mathbf{A_2}^{n-1}\mathbf{L_2}y_0 \quad (7)$$

2.2 Pole Placement

To place the observer poles, let's rearrange (7) to obtain

$$\hat{\mathbf{X}}[m+1] = \overline{\mathbf{A}}\hat{\mathbf{X}}[m] + \overline{\mathbf{B}}\mathbf{U}[m] + \overline{\mathbf{L}}y_0[m], \quad (8)$$

where $\overline{\mathbf{A}} = \begin{bmatrix} \mathbf{0} & \mathbf{0} & \cdots & (\mathbf{A_2} - \mathbf{L_2}\mathbf{C_2}) \\ \mathbf{0} & \mathbf{0} & \cdots & \mathbf{A_2}(\mathbf{A_2} - \mathbf{L_2}\mathbf{C_2}) \\ \vdots & \vdots & \ddots & \vdots \\ \mathbf{0} & \mathbf{0} & \cdots & \mathbf{A_2}^{N-1}(\mathbf{A_2} - \mathbf{L_2}\mathbf{C_2}) \end{bmatrix}$,

$$\overline{\mathbf{B}} = \begin{bmatrix} \mathbf{B_2} & \mathbf{0} & \cdots & \mathbf{0} \\ \mathbf{A_2}\mathbf{B_2} & \mathbf{B} & \cdots & \mathbf{0} \\ \vdots & \vdots & \ddots & \vdots \\ \mathbf{A_2}^{N-1}\mathbf{B_2} & \mathbf{A_2}^{N-2}\mathbf{B_2} & \cdots & \mathbf{B_2} \end{bmatrix}, \quad \overline{\mathbf{L}} = \begin{bmatrix} \mathbf{L_2} \\ \mathbf{A_2}\mathbf{L_2} \\ \vdots \\ \mathbf{A_2}^{N-1}\mathbf{L_2} \end{bmatrix},$$

$$\hat{\mathbf{X}}[m] = \begin{bmatrix} \hat{\mathbf{x}}[m,1] \\ \hat{\mathbf{x}}[m,2] \\ \vdots \\ \hat{\mathbf{x}}[m.N] \end{bmatrix} \text{ and } \mathbf{U}[m] = \begin{bmatrix} u[m,0] \\ u[m,1] \\ \vdots \\ u[m,N-1] \end{bmatrix}.$$

Poles of the observer are obtained by solving the following equation

$$\mathrm{eig}(\overline{\mathbf{A}}) = \mathrm{eig}\left(\mathbf{A_2}^{N-1}\left(\mathbf{A_2} - \mathbf{L_2C_2}\right)\right) = \left|z_2\mathbf{I} - \overline{\mathbf{A}}\right| = 0\,, \quad (9)$$

where z_2 is the Z-transform variable due to the constant sampling time T_2, *i.e.* z_2-domain.

$$z_2 = \exp(T_2 s)\,. \quad (10)$$

Solving (9), we found that there are $3N$ poles on z_2-plane. Among these, there are only 4 poles that do not locate at the origin. Hence, we can place these 4 poles to adjust the dynamics of the observer.

2.3 Verification of the Performance of the Multirate Sampling Observer

The performance of the multirate sampling observer is verified through various simulations based on the block diagram in Fig.4. The parameters of the simulations are listed in Table 1.

Fig. 5(a), (b) and (c) show the simulation results when the speed is processed by the conventional numerical differential method, the multirate sampling observer with the conventional pole placement and the multirate sampling observer with the proposed pole placement. Note that the resolution of the PG is 60 ppr, which equals to the resolution of standard PG used in Japanese trains. It is obviously seen that the response in Fig. 5(a) oscillates because of the low-resolution encoder. To improve this, the multirate sampling observer is introduced to the system. The next problem is how to adjust the dynamics of the observer. In the conventional method, the observer dynamics is adjusted by placing the pole on z_1-plane, where the interval between the pulses, T_1, at nominal speed is used as the sampling time to obtain constant observer gains. This method works effectively in middle-speed range but fail in very-low-speed range as shown in Fig. 5(b).

To solve this problem, it is necessary to consider the interval between the pulses, T_1, and the relationship of the control period, T_2, since the period of error correction is T_1, but the period of estimation is T_2. Therefore, the proposed pole placement in (9) is applied to the observer, resulting in variable gains. Fig. 5(c) shows the response according to the proposed pole placement. It is obviously seen that the stability is assured in all speed range.

3. READHESION CONTROL

The problem in readhesion control can be separated into two categories – slip-slide detection and torque adjustment. The slip-slide detection is normally implemented by comparing the wheel acceleration with a threshold. If the acceleration exceeds the threshold, the readhesion control starts and the driving or braking torque is reduced until the wheel-rail adhesion restores and the torque is increased again.

Since one-inverter-multiple-motor systems are normally implemented in Japanese train, it is impossible to control each motor independently. In this paper, we apply a one-inverter-two-motor system as an analysis model. The illustration of the train and the corresponding parameters are shown in Fig. 6 and Table 2, respectively

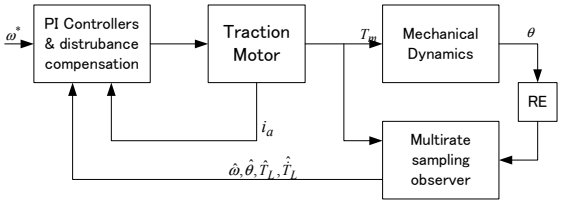

Fig. 4 Block diagram for verification of the multirate sampling observer

Table 1 Motor Parameters

Stator resistance	0.182 [Ω]
Rotor resistance	0.257 [Ω]
Stator inductance	63.44 [mH]
Rotor inductance	63.44 [mH]
Mutual inductance	63.41 [mH]
Motor and wheel inertia	15 [kgm^2]

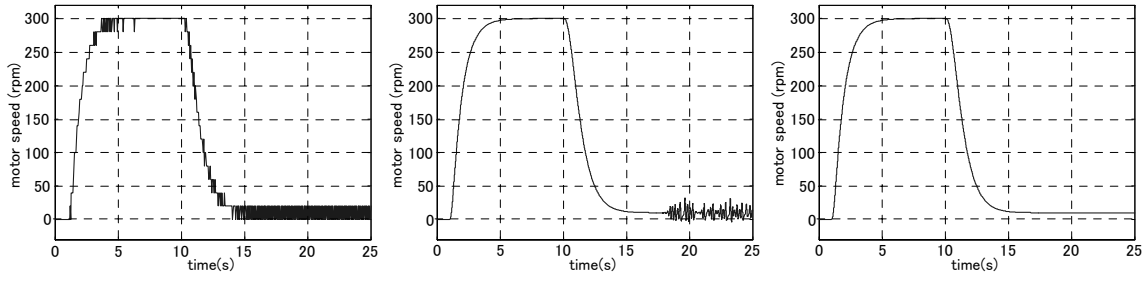

(a) (b) (c)

Fig. 5 Comparison of the numerical differentiation method and the multirate sampling observer. (a) Numerical differentiation , (b) Conventional pole placement, (c) Proposed pole placement

3.1 Slip-Slide Detection by the Multirate Sampling Observer

Since the low-resolution pulse generators are installed in Japanese train, the calculation of acceleration, of which time constant is longer that hundreds milliseconds due to the numerical differentiation, is noisy. A low-pass filter is necessary. This results in a fatal time delay for real-time slip-slide detection

The multirate sampling observer can be used for the real time estimation by using the estimated load torque as follow

$$\alpha[n] = \frac{T_m[n] + \hat{T}_L[n]}{J}, \qquad (11)$$

where J is the axle's moment of inertia. The block diagram of a one-inverter-two-motor system is shown in Fig. 7. Connection of an observer to an axle is illustrated in Fig. 8. From the block diagram, the estimated load torque implies the adhesion force. The input of the observer is the motor torque or motor current. Hence, the position of the current sensor affects the accuracy of estimation. If only one current sensor is installed at the inverter terminal, we can obtain only the average value of the current flow into each motor. For this reason, it is necessary to install current sensors at all motor terminals.

Table 2 Train's Parameters

Mass of the body, M_{body}	14000 [kg]
Mass of the bogie, M_{bg}	3000 [kg]
Mass of the axle, M_{ax1}, M_{ax2}	1500 [kg]
Spring 1 constant, k_1	10000 [kN/m]
Spring 2 constant, k_2	8000 [kN/m]
Damper 1 constant, b_1	100 [kN/m/s]
Damper 2 constant, b_2	80 [kN/m/s]
Front wheel diameter r_1	430 [mm]
Rear wheel diameter, r_2	427 [mm]
Gear ratio, R_g	5.31

When slip-slide occurs, the motor torque and the axle's moment of inertia are constant. Therefore, we can theoretically detect slip-slide by using the estimated load torque. In practice, however, the estimated load torque includes the effect of slope so when the train runs into a down slope, the level of the estimated load torque increased, as well as the acceleration. If the threshold is set at a small value, the slip-slide is detected and the readhesion control starts although the train still runs in normal condition. Therefore, the parameter that does not include the effect of slope is desirable. For this reason, we introduce a parameter called "the amount of the load torque correction" which is defined as

$$\Delta\hat{T}_L = \hat{T}_L[N] - \hat{T}_L[N-1]. \qquad (12)$$

This parameter can be obtained only when the pulse is detected. Fig. 9 shows the calculation of this parameter. Comparison of each parameter is shown in Fig.10. Note that the 1% down slope is assumed and the slip-slide

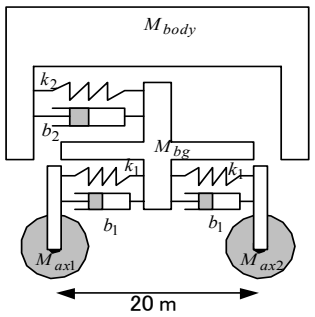

Fig. 6 Two-axle bogie model

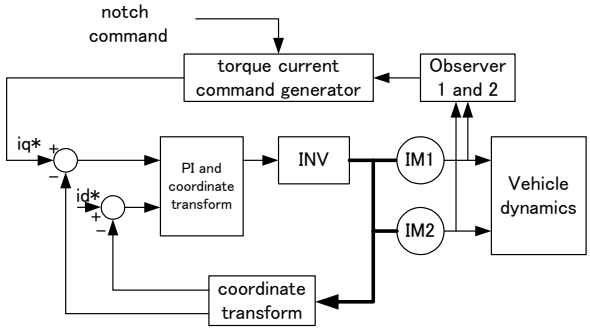

Fig. 7 Block diagram of a one-inverter-two-motor System

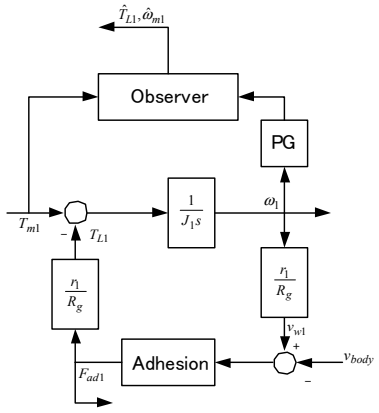

Fig. 8 Connection of the observer

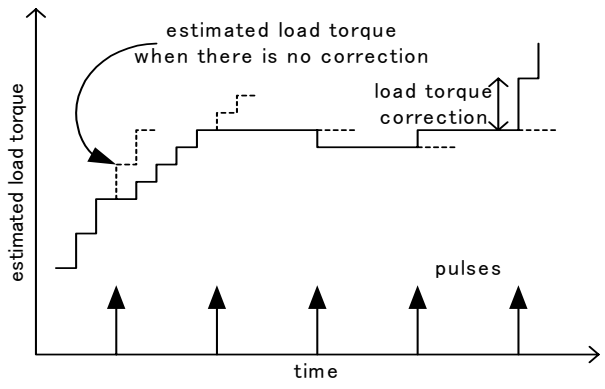

Fig. 9 Calculation of the amount of the load torque correction

occurs at the 14th second. It is obviously seen that the acceleration calculated directly from the pulses is very noisy, whereas the acceleration calculated by (11) is not, as well as the estimated disturbance. However, there is an offset due to the slope. Conversely, the amount of the load torque correction has no offset due to the slope. This signal, therefore, is more suitable for slip-slide detection than the estimated disturbance itself.

3.2 Torque Adjustment

When the slip-slide occurs, it is necessary to reduce the motor torque in order to restore the adhesion between the rail and the wheels. In case of one-inverter-multiple-motor driving system, each motor cannot be controlled independently. Therefore, when one axle slips, the torque of all related axles is reduced. The torque is normally reduced to a suitable value based on experience. In fact, the amount of the reduce torque should relate to the amount of the adhesion force for fast restoration the adhesive condition without excessive acceleration or deceleration drop. For this reason, we propose a novel torque adjustment method by using the estimated load torque force from the multirate sampling observer, which has close relationship with the adhesion force.

Since it is necessary to consider the effect of the bogie's moment of inertia, the amount of the load torque that used for torque adjustment is not the instantaneous value but the average value during 0.2 second before the slip-slide occur. In this paper, we reduce the torque to 50% of this average amount after slip-slide detection. Note that the thresholds for slip-slide detection and recovery are proportional the motor's angular speed by the relation in (13) and (14), respectively.

$$\Delta T_{L-TH1} = 0.03\omega \tag{13}$$

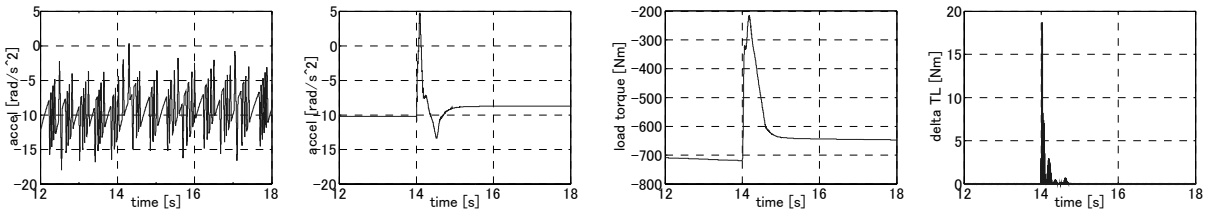

(a) (b) (c) (d)

Fig.10 Comparison of parameters used for slip-slide detection. (a) Acceleration calculated by the conventional method, (b) Acceleration calculated by the estimated load torque, (c) Estimated load torque, (d) Amount of the Load torque correction

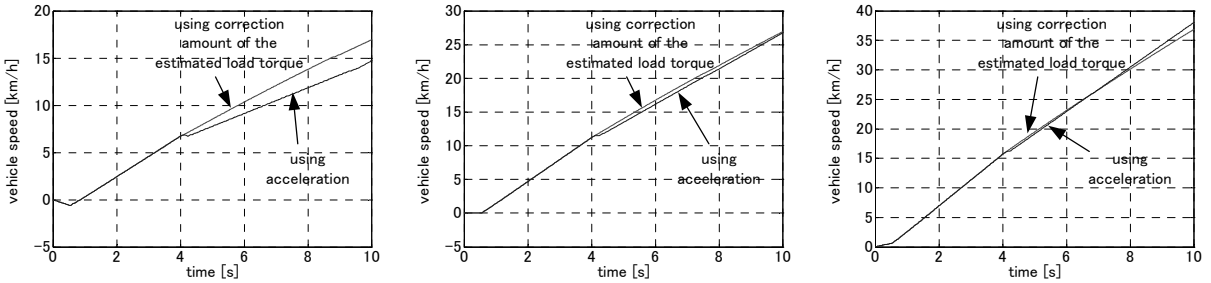

(a) (b) (c)

Fig.11 Simulation results during acceleration.
(a) Up slope 4% (b) No slope (c) Down slope 4%

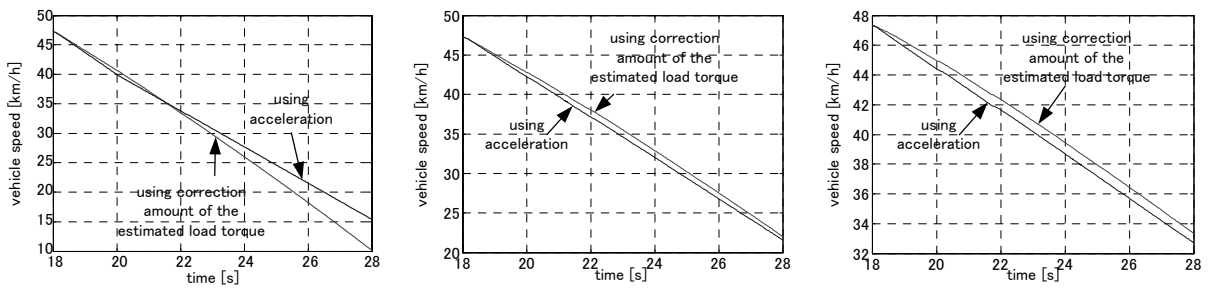

(a) (b) (c)

Fig.12 Simulation results during braking.
(a) Up slope 4% (b) No slope (c) Down slope 4%

$$\Delta T_{L-TH2} = 0.005\omega \quad (14)$$

When the amount of the load torque correction drop below the recovery threshold, the adhesive condition is restored and the motor torque is increased again.

Fig. 11 shows the effect of the slope to each readhesion control method during acceleration. The train runs into the slippery region at the 4th second. Note that in the conventional method, using the acceleration for slip-slide detection, the threshold is set to 20 and 10 rad/s^2, respectively and the torque is reduce to 50% of the command. It is obviously seen that the proposed method, using amount of the load torque correction for slip-slide detection, works effectively at any slope condition. On the other hand, the thresholds in the conventional method are sensitive to the slope and the torque adjustment is fixed. This cause the excessive drop of the torque current, which finally results in small acceleration as shown in Fig. 11(a).

The effect of the slope during braking is shown in Fig. 12. The train runs into the slippery region at the 20th second. The proposed algorithm causes a small deceleration when starting braking because the estimated load torque changes when the torque command abruptly changes. The amount of the load torque is greater than the threshold resulting in reduction of the torque current. However, the deceleration increases gradually and it is insensitive to the effect of the slope, as well as the acceleration mode. On the other hand, the convention readhesion control is sensitive to the slope.

4. CONCLUSIONS

This paper has described an effective way to improve readhesion control of a train in which low-resolution pulse generators are installed. The multirate sampling observer, which solves the problem of low resolution, has been introduced. The simulation results have shown that the multirate sampling observer can improve the speed and acceleration estimation.

Two multirate sampling observers have been then applied to the axle for readhesion control. The amount of the load torque correction from the observers has been used as the slip-slide detection parameter. This parameter is insensitive to the geographical profile of the track, unlike the acceleration, which is conventionally used for the slip-slide detection. Therefore, it can solve the problem of threshold selection. For fast restoration the adhesive condition without excessive acceleration or deceleration drop, moreover, we proposed a novel torque adjustment method by using the estimated load torque force from the multirate sampling observers, which has close relationship with the adhesion force, since the amount of the reduce torque should relate to the amount of the adhesion force. The simulation results confirm the effectiveness of this method.

REFERENCES

[1] Sone, S.: Power Electronic Technologies for Low Cost and Energy Conservation on World Railways Vehicles, *Proc. IPEC-Tokyo2000*, vol.1, pp. 452-457, 2000.
[2] Hori Y.: Robust Motion Control Based on a Two-Degrees of-Freedom Servosystem, *Advanced Robotics*, vol.7, No.6, pp.525-546, 1993
[3] Araki M, Yamamoto M.: Multivariable Multirate Sampled-Data System: State-Space Description, Transfer Characteristics and Nyquist Criterion, *IEEE Trans. Automatic Control*, vol. AC-31, pp.145-154, 1986.
[4] Watanabe T.: Anti-Slip/slide Readhesion Control Problem of Electric Railway Vehicle, *Proc. 2002 Japan Industry Application Society Conference*, vol. 1, pp.259-262, 2002 (in Japanese).
[5] Tateishi D., Kovudhikulrungsri L., Koseki T.: The Influence of Bogie Vibration upon Readhesion Control, *Proc. 2002 Japan Industry Application Society Conference*, vol. 1, pp.271-274, 2002 (in Japanese).
[6] Kovudhikulrungsri L., Koseki T.: Precise Torque and Speed Control In Pure Electric Braking Operation of AC Traction in Low Speed Range, *International Workshop on Advance Motion Control*, pp.142-147, Maribor, Slovenia, Jul., 2002
[7] Kovudhikulrungsri L., Koseki T.: Control of a Traction Motor at Low Speed with Consideration of Vehicle Dynamics, *Transportation, Electric Railways and Linear Drive Conference*, pp.35-40, Kokura, Japan, Jul., 2002
[8] Kovudhikulrungsri L., Tateishi D., Koseki T.: Parameter Estimation by Multirate Sampling Observer for Slip-slide Detection, *2003 IEEJ National Convention Record*, Vol.5, pp.304-305, Sendai, Japan, Mar, 2003 (in Japanese)